# SPIN-LATTICE RELAXATION TIME OF COLOUR CENTRES IN QUARTZ

by

Shu-teh Wang

# SPIN-LATTICE RELAXATION TIME OF COLOUR CENTRES IN QUARTZ

by

Shu-teh Wang

A thesis submitted to the Faculty of Graduate Studies
and Research in partial fulfillment of the requirements
for the degree of Master of Science

Eaton Electronics Research Laboratory
Department of Physics
McGill University
Montreal, Quebec

March 1965

Contents

## Acknowledgements

The author wishes to express his sincere gratitude to Professor G. W. Farnell, research director, for his constant guidance and encouragement throughout this research.

The author is also grateful to Mr V. Avarlaid, Supervisor of Technical Services of the Eaton Electronics Research Laboratory, and his staff, for their assistance in the laboratory work.

The generous assistance of Mr Y. L. Wang of the Department of Mechanical Engineering, in the preparation of the computer programme, and Miss L. Farquharson in careful reading of the manuscript, are also gratefully appreciated.

This research was supported by the National Research Council and the Defence Research Board through grants to the Eaton Electronics Research Laboratory. Such financial assistance is also gratefully acknowledged.

## Abstract

Spin-lattice relaxation times of X-cut quartz, irradiated by 1 Mev electrons, were measured by means of the saturation technique. Measurements were made in the temperature range from 1.6°K to 4.2°K for four different concentrations, and the values of $T_1$ were found to obey a $T_1 \propto T^{-0.7}$ law below 3°K, and a $T_1 \propto T^{-3}$ law above 3°K.

Measurements of the $T_1$ dependence on concentration were also carried out. These experimental results were fitted to an empirical formula by means of the method of least squares. The empirical formula is

$$T_f\,(\text{sec.}) = 0.198^2 + 0.164 \times 10^1 c_s - 0.119 \times 10^2\, c_s^2 + 0.262 \times 10^2 c_s^3 - 0.246 \times 10^2\, c_s^4 + 0.848 \times 10^1\, c_s^5$$

where $c_s$ is in unit of $4 \times 10^{19}$ spins/c.c.

At the highest concentration the relaxation time was 10 ms at 4.2°K.

# I. Introduction

Langevin's classical theory of paramagnetism postulates magnetic substances as assemblies of isolated magnetic dipoles, which, in the absence of magnetic field are distributed in random directions, and show no magnetic moment. No consideration is given to the re-distribution of the isolated dipoles during the period immediately after an external magnetic field is applied. After the application of such a field, a definite time interval, however small, is required for these magnetic dipoles to establish a state of equilibrium; and the length of this interval depends on the magnetic forces tending to orient the dipoles in the direction of the applied magnetic field, on the random forces of thermal agitation, and on the constraints arising from the interaction of the dipoles with their surroundings and with each other. According to whether the applied field is weak or strong as compared with the internal field of the magnetic ions, two kinds of characteristic relaxation time may be defined. In the former case, the relaxation effects depend only on spin-spin interaction and the relaxation time is of the order of $10^{-10}$ second.

In a small magnetic field, the states of electron spins are distributed in accordance with Boltzmann's statistics. If the sample is suddenly put into a large magnetic field, the spins will seek to obtain a new thermal equilibrium state, characterized by a small excess of spins in the lower energy states, and, for this to occur, spins must make transitions to the lower energy states by one means or another. Interactions of spins with the crystal lattice can affect these transitions, the characteristic time required for the excess energy to be given to the

lattice being called the spin-lattice relaxation time $T_1$.

The first theoretical paper about spin-lattice relaxation times in solids was given by Waller (1932), who considered the modulation of the internal dipolar field by lattice vibrations in detail, and found the spin-lattice relaxation time $T_1$ to be dependent on temperature. However, the value for the relaxation time obtained by Waller is much greater than the true value, since he neglected interaction between the individual spins and the lattice vibrations. Waller also pointed out that two types of processes must be considered, which are the direct absorption or emission of a quantum of lattice vibration by the spin system, and the inelastic scattering of the lattice vibrations by the absorption of one quantum and the emission of the other of different energy. The first type of process is the so-called direct process and the second which is especially important at high temperature, and which can be compared with the Raman process in optics, is called the Raman or indirect process.

In their treatment of magnetic cooling, Heitler and Teller (1936) pointed out that the magnetic energy of the spin must be transferred to the lattice vibrations. Since the spin energy levels are influenced by the static effects of the electric field of the crystalline lattice, the variations of the electric field due to thermal vibration provide a perturbation capable of inducing transitions. Heitler and Teller were thus able to derive a formula for $T_1$ dependent on temperature. Using the same modulating crystalline electric field through lattice vibrations, Fiez obtained an expression for the Raman process. The calculations of these workers, however, showed that the crystalline electric field modulation mechanism was inadequate to account for the observed relaxation time.

Kronig (1939) suggested that the relaxation time, $T_1$, influenced

by the modulation of the crystalline electric field due to lattice vibration, might arise from the spin-orbital coupling. When the lattice vibrates, the orbital motion in the magnetic ion undergoes periodic changes due to the variations in the electric field of the crystal, and these changes react on the spin through spin-orbital coupling, causing them to alter their orientation with respect to the applied D. C. magnetic field. Kronig obtained an order of magnitude expression for ions of $S = \frac{1}{2}$ which agreed fairly well with experimental results.

One year later, Van Vleck (1940), using the spin-orbital coupling mechanism, which he worked out independently, found that, under precise consideration, Kronig's results were not entirely satisfactory. Van Vleck worked explicitly on $Ti^{3+}$ and $Cr^{3+}$ ions in alums with the consideration of the vibrations of the surrounding complex of six water molecules, but his values for the spin-lattice relaxation time were also longer than the observed values in the liquid helium temperature range.

More recently, Mattuck and Strandberg (1960), modified Van Vleck's method of calculation, using a more general method, and obtained the same result. They pointed out that Van Vleck chose the wrong initial and final state of transition and also grouped the perturbation Hamiltonian incorrectly. Even if equivalent results had been obtained by these different authors, their results differed in higher order perturbations. Orbach (1961) proposed a different mechanism for the rare-earth group ions. In most rare-earth salts, the crystalline electric field splittings of the ground multiplet are small compared with the available phonon energies, so that direct phonon-induced transitions can take place between the different states. This can be furthermore explained as follows; the ground states

of a given rare-earth salt are denoted by $|b\rangle$ and $|a\rangle$, where $|b\rangle$ is the upper ground state. In addition, $|c\rangle$ is an excited state in which the energy splitting with the ground states is less than the maximum energy of the phonons. An ion in state $|b\rangle$ absorbing a phonon, will transform to state $|c\rangle$, then in a second step, the ion will emit a phonon of different energy from the previously absorbed phonon, making a transition back to state $|a\rangle$.

It has been pointed out that Kronig and Van Vleck, using the modulation of a crystalline electric field, instead of a magnetic field, due to thermal lattice vibration as perturbation, found order-of-magnitude values. However, in F-centre crystals, the modulation of the internal magnetic dipolar field is also important in first order perturbation as well. This occurs because the F-centre electrons have a relatively large hyperfine coupling to the nuclei, which surround the hole. Therefore, the transitions between the allowed Zeeman splittings should include the nuclear spin quantum number $m_I$ and the electron spin quantum number $m_S$. Spin-lattice relaxation times are usually associated with those transitions which satisfy the selection rules $\Delta m_I = 0$, $\Delta m_S = \pm 1$.

The reasons for using smoky quartz for spin-lattice relaxation time measurements here are based on the following:

1. Since different quartz crystals have various concentrations of aluminum impurity, a given quartz crystal can provide any desired number of colour centres up to a limit.

2. The electron-spin-resonance absorption spectra of the smoky quartz have been extensively investigated.

3. Measurements on spin-lattice relaxation time have already been made at temperatures 4.2°K and 1.6°K for several concentrations.

4. Measurements, other than spin-lattice relaxation, such as spin-phonon interaction, dielectric loss etc., have been extensively carried out. Models, which explain the experimental results satisfactorily, were proposed by O'Brien (1955) and Taylor (1963). There are still conflicts existing about the relaxation mechanism, but further experimental results may give information with which an adequate mechanism may be constructed.

The spin-lattice relaxation time measured by Carr and Strandberg (1962) was about 10 times longer than that measured by Taylor (1963). This discrepancy cannot be attributed to experimental errors. Since cross-relaxation may play an important role in smoky quartz, the spin-lattice relaxation time was measured here at varying concentrations. Taylor proposed that the spin-lattice relaxation follows neither the usual direct process at very low temperature nor the Raman process at higher temperature. But Shamferov and Smirnova (1963) reported that they had found the existence of both the direct and the Raman processes when they used neutron-irradiated quartz. Even Taylor's own experiment showed the likelihood of the two processes being present. In order to clarify this, experiments on the temperature dependence of spin-lattice relaxation time were carried out in the range from 4.2°K to 1.6°K. All experimental procedures and results will be presented in chapters V and VI.

## II. Quartz Crystallography and Smoky Quartz

### A. Quartz Crystallography

Quartz, also called silicon dioxide, is one of the commonest minerals to be met with in a great variety of forms, of which α-quartz, crystallized below 573°C is the most common. α-quartz has neither plane nor centre symmetry, but three two-fold axes perpendicular to the principal triad axis. Hence, in crystallography, it belongs to the space group $D_3^4$ and $D_3^6$ (see figure 1). The majority of quartz crystals are bound by faces of a hexagonal prism and a hexagonal bipyramid as shown in figure 2a, although the prism is sometimes absent. The z-axis of quartz is in the direction of the principal triad axis, whereas the x-axis and y-axis are in the plane, in which one of the two-fold axes is usually referred to as y-axis, perpendicular to the z-axis (figure 2b).

The unit cell of quartz is in the form of a right prism of height c, and with a 60° rhomboidal base of sides a and b. There are three $SiO_2$ molecules in one unit cell, in which one of those silicon atoms is on the two-fold axis located at a distance c/3 above the base, surrounded by four oxygen atoms to form an irregular tetrahedron. The distances between two oxygen atoms are 2.62 Å, 2.64 Å, 2.60 Å, and 2.67 Å, and those between an oxygen atom and a silicon atom are 1.61 Å, 1.62 Å, 1.60 Å, 1.62 Å. The angle made by oxygen atoms to the silicon atom is 144° (Wei, 1935).

### B. The Colour Centres

Natural ∝-quartz usually contains impurities such as aluminum, sodium etc. According to O'Brien (1955) the smoky quartz spectrum

described by Griffiths (1954) may be attributed to the aluminum impurity. In silicon dioxide, each silicon atom of valence four, forms four co-valent bonds with the oxygen atoms. Thus, there are twelve co-valent bonds in one unit cell, all of the same kind, although the surroundings of the oxygen atoms are different. The aluminum atom, having merely three valence electrons, can only form plane or pyramidal bonds. However, by accepting an extra valance electron, the aluminum atom can also form a tetrahedral bond. Thus, by accepting an extra electron from the 2p shell of the oxygen atom, the aluminum atom can replace the silicon atom in quartz. In order to maintain electrical neutrality, each $Al^-$ ion must be accompanied by a positive ion such as $Na^+$ or $Li^+$. After irradiation, the positive ion captures an electron to became neutral, and the tetrahedrons formed by Al-O bonds are completed. The missing orbital electrons from the oxygen atoms will act as paramagnetic centres.

The spectrum of smoky quartz was fitted by O'Brien to the spin Hamiltonian

$$\mathcal{H} = \beta \vec{H} \cdot g \cdot \vec{S} + A_{z'} I_z S_{z'} + A_{x'} I_{x'} S_{x'} + A_{y'} I_{y'} S_{y'} + P\left[I_{z'}^2 - \tfrac{1}{3} I(I+1)\right] - \gamma \beta_n \vec{H} \cdot \vec{I}$$

where $S = 1/2$ $\quad I = 5/2$ (II-1)

$g_{11} = 2.06$ $\quad g_{\perp} = 2.00$

$A_{z'} = 4.8 \times 10^{-4}$ cm$^{-1}$ $\quad A_{x'} = A_{y'} = 5.5 \times 10^{-4}$ cm$^{-1}$

$P = -0.4 \times 10^{-4}$ cm$^{-1}$

The g-tensor has axial symmetry, with the axis of each centre approximately parallel to the line joining a pair of silicon atoms. The hyperfine

structure is attributed to the aluminum ($I = 5/2$), and its axes $x'$, $y'$, $z'$ are not the same as the axes of g-tensor.

An aluminum atom can replace any of the three silicon atoms in one unit cell, so that there may be twelve Al-O bonds in total, and theoretically, each oxygen atom can supply an orbital electron to form colour centres. In actual fact, unexplicably, this does not happen, and only six possible sites for the formation of colour centres can be identified from observations.

From the results of cross-relaxation and dielectric loss measurements, Taylor proposed that under the influence of thermal agitation of lattice vibrations, the hole at a given aluminum impurity can move back and forth between the two oxygen orbitals, and it is also possible for the hole to jump from one oxygen atom to another (Taylor and Farnell, 1964). The latter mechanism leads to the term of so-called site-to-site relaxation.

The smoky quartz electron-spin-resonance absorption spectra are very complicated. There are six lines in a group, which may be contributed from the site of the aluminum impurity ($S = 1/2$, $I = 5/2$). In addition, many smaller lines have been observed, these perhaps being due to the forbidden transitions in which $\Delta m \geq 1$ (Griffiths et al, 1955).

## III. Theory of Spin-lattice Relaxation Time

A paramagnetic centre in a crystal lattice will be affected by an electric field which is formed by the neighbouring ions, and when the lattice vibrates, the interionic distances are modulated at the frequency of lattice vibrations. The crystalline electric field is modulated and gives a perturbation to the original Hamiltonian to produce spin transitions by means of spin-orbital interaction. On the other hand, an oscillating magnetic field component arising from the motion of the magnetic dipoles, will also give a perturbation effect.

For a paramagnetic centre, the Hamiltonian of the electron-lattice system may be written in the form

$$\mathcal{H} = \mathcal{H}_e + \mathcal{H}_i \qquad \text{(III - 1)}$$

where $\mathcal{H}_e$ is the Hamiltonian containing the static interaction of an electron with the external magnetic field and the lattice, $\mathcal{H}_i$ is the Hamiltonian which contains the interaction between the centres and the lattice vibrations. The observed electron-spin-resonance absorption spectra corresponds to transitions among the lowest lying eigenstates of $\mathcal{H}_e$.

$\mathcal{H}_e$ is given by Feldman et al (1964) as

$$\begin{aligned}\mathcal{H}_e = \frac{p^2}{2m} + e\phi(\vec{r}) + \beta\vec{H}\cdot(\vec{L}+2\vec{S}) + \lambda\vec{L}\cdot\vec{S} + \sum A_k \vec{S}_k\cdot\vec{I} \\ + \sum_k \frac{B_k}{r_k^3}\left[3\frac{(\vec{I}_k\cdot\vec{r}_k)(\vec{S}\cdot\vec{r}_k)}{r_k^2} - \vec{I}_k\cdot\vec{S}\right] \\ + \sum_l \frac{C_l}{r_l^2}\left[3\frac{(\vec{S}_l\cdot\vec{r}_l)(\vec{S}\cdot\vec{r}_l)}{r_l^2} - \vec{S}_l\cdot\vec{S}\right] \qquad \text{(III-2)}\end{aligned}$$

where $\phi(\vec{r})$ is the electrostatic potential produced by the lattice ions surrounding the paramagnetic centre; $\lambda$ is the spin-orbital coupling coefficient; $A_k$ is the isotropic hyperfine coupling coefficient for the k-th nucleus; $B_k$ is the anisotropic hyperfine coupling coefficient for the k-th nucleus and $C_\ell$ is the coupling coefficient for the dipolar interaction of the centre with the l-th identical neighbouring centres.

According to Orbach (1961), the Hamiltonian $\mathcal{H}_i$, contributed from the interaction between the paramagnetic centre and lattice vibrations, can be expanded into a power series in terms of the strain produced at the paramagnetic centre by the phonons. Thus we have,

$$\mathcal{H}_i = \sum_m V_m \epsilon_m + \sum_{m,n} V_{mn} \epsilon_m \epsilon_n + \cdots \qquad \text{(III-3)}$$

where $\epsilon_m$ is the strain produced by a phonon in the m-th mode, and

$$V_m \equiv \frac{\partial \mathcal{H}_e}{\partial \epsilon_m} \qquad V_{mn} \equiv \frac{\partial^2 \mathcal{H}_e}{\partial \epsilon_m \partial \epsilon_n} \qquad \text{(III-4)}$$

Since $\epsilon_m$ is time-dependent, $\mathcal{H}_i$ is likewise, and exchange of energy will occur between the spin system and the lattice. The time required for energy to be transferred from the spin system to the lattice to reach thermal equilibrium is the spin-lattice relaxation time $T_1$.

Two kinds of mechanism, which depend on the crystalline field interaction and magnetic dipole-dipole interactions, may occur simultaneously or one at a time. That transitions are contributed by the modulation of crystalline electric fields through the spin-orbital coupling, has been widely accepted since Kronig introduced this idea in 1939. However, the mechanism arising from dipole-dipole interaction has not been similarly regarded, even though it was introduced seven years earlier.

In order to calculate the spin-lattice relaxation time, it is necessary to find the transition probability per unit time for an electron spin flipping from a state $|b\rangle$ to a state $|a\rangle$. Since the Raman, or indirect, process in which a spin flip is accompanied by the inelastic scattering of a phonon, results from non-linear term in $\mathcal{H}_i$ taken to the first order, and from the linear term in $\mathcal{H}_i$ taken to the second order in the perturbation theory, we will consider only the order up to two in the following.

The probability per unit time for an electron spin making the transition between states $|b\rangle$ and $|a\rangle$ by the time-dependent Hamiltonian $\mathcal{H}_i$ is (Heitler, 1944),

$$W_{b\to a} = \frac{2\pi}{\hbar} |\langle a|\mathcal{H}_i|b\rangle|^2 \rho(E) \qquad \text{(III-5)}$$

where $\rho(E)$ is the density of the final states.

The direct process, in which an electron spin flip is accompanied by the absorption or emission of a resonant phonon, occurs when the first order time-dependent perturbation theory is applied to the linear term in the equation (III-3). Thus,

$$W_{b\to a} = \frac{2\pi}{\hbar} |\langle a|\sum_m V_m \epsilon_m|b\rangle|^2 \rho(E) \qquad \text{(III-6)}$$

and the corresponding transition probability for the Raman process is

$$W_{b\to a} = \frac{2\pi}{\hbar} \left| \sum_j \frac{\langle a|\sum_m V_m \epsilon_m|j\rangle\langle j|\sum_n V_n \epsilon_n|b\rangle}{E_a - E_j} + \langle a|\sum_{mn} V_{mn}\epsilon_n\epsilon_m|b\rangle \right|^2 \rho(E)$$

Since $\lambda$, the spin-orbital coupling coefficient, depends on the relative positions of the hole and its neighbouring nucleus, $r$, the lattice

vibration makes the spin-orbital coupling time-dependent. Thus the time-dependent crystalline electric field causes transitions within the ground state multiplet. The hyperfine coupling coefficient $A_k$, also depends on $\vec{r}$, and the first order perturbation of $A_k$ has non-vanishing matrix elements of $S_+ S_-$, leading to transitions of the type $\Delta m_S = \pm 1$, $\Delta m_I = \mp 1$, in which electron and nucleus flip in opposite directions.

The time-dependent anisotropic hyperfine coupling coefficient $B_k$, by first order perturbation, leads to non-vanishing matrix elements $S_z S_\pm$, $S_z I_\pm$, $S_\pm I_\mp$, and $I_\pm S_\mp$. This means that electron and nucleus can flip separately or that both can flip simultaneously. Finally, the electron-electron interaction term, in which the one containing $\vec{S}_1 \cdot \vec{S}$ leads to mutual flips of a pair of spins, does not lead to spin-lattice relaxation. The other term does give rise to spin-lattice relaxation, but its contribution can be made insignificant by sufficient dilution of the paramagnetic centres.

Because of its complexity, we will abandon the anisotropic property of elastic wave propagation in solids, and assume that the strain in equation (III-3) can be represented by the average value $\epsilon$, at the mean time. The expression of $\mathcal{H}_i$ in equation (III-3) is evaluated at $\vec{r}_o$, such that $V_m$, $V_{mn}$, etc., are time-independent, so that we obtain a simpler expression for

$$\mathcal{H}_i = A\epsilon + B\epsilon^2 \qquad \text{(III-3a)}$$

The density of final states is (Abragam, 1961),

$$\rho(E) = \frac{3\omega^2}{2\pi^2 v^3} \qquad \text{(III-8)}$$

where v is the propagation velocity of an elastic wave in the lattice.

Equation (III-6) can thus be written,

$$W_{b\to a}=\frac{2\pi}{\hbar}\int A^2\left|\langle a|\epsilon|b\rangle\right|^2\frac{3\omega^2}{2\pi^3 v^3}\,\delta(E-E_o)\,dE \qquad \text{(III-9)}$$

where $\delta\,(E - E_o)$ means that possible transitions are from the states of eigenvalue E to those of eigenvalue $E_o$ only.

The matrix elements of the strain, $\epsilon$, at a point $\vec{r}$ for a particular mode k of occupation number N, are (Ziman, 1960)

$$\langle N+1|\epsilon|N\rangle = k\left[\frac{\hbar(N+1)}{2M\omega}\right]^{\frac{1}{2}} e^{-i\vec{k}\cdot\vec{r}}$$

$$\langle N-1|\epsilon|N\rangle = k\left[\frac{\hbar N}{2M\omega}\right]^{\frac{1}{2}} e^{i\vec{k}\cdot\vec{r}} \qquad \text{(III-10)}$$

These elements correspond to the creation and destruction of a phonon of energy $\hbar\omega$ appropriate to the transition we have considered.

From equation (III-9), the probability of transitions from state $|b\rangle$ to state $|a\rangle$ is

$$W_{b\to a}=\frac{3A^2}{2\pi v^5\hbar}\,\frac{\omega^3}{M}\,N_b(N+1) \qquad \text{(III-11)}$$

where N is the number of phonons of mode k. Since a phonon satisfies Bose-Einstein statistics,

$$N=\frac{1}{e^{\frac{\hbar\omega}{kT}}-1} \qquad \text{(III-12)}$$

Now, we are going to evaluate the reverse probability, which is the transition from state $|a\rangle$ to state $|b\rangle$.

$$W_{a\to b}=\frac{3A^2}{2\pi v^5\hbar}\,\frac{\omega^3}{M}N_a N \qquad \text{(III-13)}$$

The net transition probability going from state 1b> to state 1a> is equal to the difference of $W_{b \to a}$ and $W_{a \to b}$.

Thus

$$-\frac{dN_b}{dt} = \frac{3A^2\omega^3}{2\pi v^5 \hbar M}\left[N_b(N+1) - N_a N\right] \qquad \text{(III-14)}$$

If $n = N_b - N_a$, and $N_a + N_b = N$, and since the number of phonons of mode k in the system is constant,

$$\frac{dn}{dt} = -\frac{3A^2}{2\pi M \hbar v^5}\omega^3 \coth\frac{\hbar\omega}{2KT}(n - n_o) \qquad \text{(III-15)}$$

where $n_o = N^2 \tanh\frac{\hbar\omega}{2KT}$.

The solution of equation (III-15) is

$$n = n_o e^{-\frac{t}{T_1}} \qquad \text{(III-16)}$$

where

$$\frac{1}{T_1} = \frac{3A^2\omega^3}{2\pi v^5 M \hbar}\coth\frac{\hbar\omega}{2KT} \qquad \text{(III-17)}$$

and $T_1$ is the spin-lattice relaxation time.

In the case $\hbar w << KT$, the energy splittings are much smaller than the thermal energy, and $\coth\frac{\hbar\omega}{2KT}$ can be expanded in terms of $\frac{\hbar\omega}{2KT}$ and higher order terms neglected.

$$\frac{1}{T_1} = \frac{3A^2\omega^2}{\pi\hbar^2 M v^5} KT \qquad \text{(III-18)}$$

Thus $T_1$ is proportional to T for the direct process.

Using the theory of conservation of energy, $E' - E = \hbar\omega_o$, thus the frequency difference of the absorption and emission phonons in a Raman process is equal to the frequency of the scattering phonon, $\omega' - \omega = \omega_o$. However, since $\omega_o$ is much smaller than either $\omega'$ or $\omega$, we

obtain from equation (III-7), that the transition probability per unit time from state |b⟩ to state |a⟩ is,

$$W_{b\to a} = \frac{9}{8\pi^3 M^2 v^{10}} N_b \left\{ \int \frac{A^4 \omega^6 N(N+1)}{\hbar\omega - \Delta} d\omega + \int B^2 \omega^6 N(N+1) d\omega \right\} \qquad \text{(III-19)}$$

Since the elastic constants A and B are of the same order of magnitude and are usually much smaller than 1, the first term of equation (III-19) is negligible compared to the second term. Thus, after a calculation equivalent to those used in equations (III-11) and (III-13), we get,

$$\frac{1}{T_1} = \frac{9B^2}{8\pi^3 M^2 v^{10}} \omega_0^7 \left(\frac{T}{\theta}\right)^7 \int_0^X \frac{e^x x^6}{(e^x - 1)^2} dx \qquad \text{(III-20)}$$

where $x = \frac{\hbar\omega}{KT}$, $X = \frac{\hbar\omega_0}{KT}$, $\omega_0$ is the Debye frequency of the lattice, and $\theta$ is the Debye temperature defined by $K\theta = \hbar\omega_0$.

For $T \ll \theta$, the integral in equation (III-20) tends toward a limiting value independent of T. Thus, the spin-lattice relaxation time, $T_1 \propto T^{-7}$. It should be noted that the integral converges rather slowly, and the $T_1 \propto T^{-7}$ law is only valid when $\frac{T}{\theta} \leq 0.02$ (Abragam, 1961). For $T \gg \theta$, $e^{\frac{\hbar\omega}{KT}}$ can be expanded into $1 + \frac{\hbar\omega}{KT}$, the spin lattice relaxation time $T_1 \propto T^{-2}$.

## IV. Apparatus

The X-band heterhedrodyne spectrometer used in this experiment is similar to that discussed by Feher (1957) modified by the addition of two precision micro-wave attenuators immediately before and after the magic T bridge as described in detail by Lortie (1960).

The micro-wave power is supplied by a Pounder stabilized Sperry 2K39 klystron with frequency stability better than two parts in $10^7$ at frequency 9400 Mc/sec. A magic T with one arm leads to the micro-wave source, which is attenuated by a 50 db variable attenuator to keep the power leading to the cavity, forming another arm of the magic T, at a desired level. The reflection power from the cavity, containing the signal, leads to a balanced mixer through another 50 db variable attenuator. This signal modulated by micro-wave power from a local oscillator of frequency 30 Mc/sec. off the frequency of the main micro-wave source, was lead to the detector system and displayed on a recorder. By proper adjustment of the two variable attenuators, the signal level incident on the crystal mixer can be kept constant, while the power incident on the sample varies over a wide range. A variable phase shifter and attenuator form the "dummy arm" of the magic T.

The Pacific 12" magnet gives a short time stability of one part in $10^4$. A 200 cycles/sec. audio-frequency magnetic field is produced, parallel to the D.C. magnetic field, by adding two Helmholtz coils at both magnet poles. The effect of the magnetic field modulation is to modulate the micro-wave signal reflected from the cavity at 200 cycles/sec. The signal amplitude is proportional to the derivative of the magnetic susceptibility.

In order to establish magnetic resonant conditions, one can either change the frequency of the power source or the magnitude of the D. C. magnetic field. The latter method has been found to be more convenient.

The reflected signal is actually a function of the derivatives of $\chi'$ and $\chi''$, but in all of the experiments described here, the $\chi'$ component is eliminated. By suitable adjustments of the variable phase shifter and attenuator on the "dummy arm", the bridge can be balanced to a null condition off resonance. When magnetic resonance is obtained, the changes in $\chi''$ of the sample unbalance the bridge, causing a net reflected signal to be sent into the detector system.

During the later part of this work, the local oscillator was stabilized at 9400 Mc/sec., and simultaneously, a narrow band pass filter was placed immediately before the mixer. This improved the signal to noise ratio about three times.

## V. Measurement Techniques

### A. The Sample

A 1.5 cm. long, 0.3 cm. in diameter, X-cut natural quartz crystal, was irradiated by 1 Mev electrons from a linear accelerator until it became opaque, that is saturated. This crystal was mounted parallel to the magnetic field through the centres of the broad surfaces of the rectangular cavity, which was originally designed for accoustic absorption purpose, as reported by Taylor (1963). Since the direction of the x-axis of the quartz is fixed, only one parameter is to be changed, unlike that of the sample placed on the plunger which has two parameters to be changed. This reduces the work for mounting.

Once a given crystal was mounted in the cavity the spectral lines for a given site could be resolved for only a small angular range of D.C. magnetic field. Also because the sensitivity of the spectrometer depends on the angle of the cavity with respect to the D.C. field, the angular range for spin-lattice relaxation purposes is quite limited. In this thesis, all the experiments were carried out on the transition (1/2, 3/2→1/2, 3/2) and sometimes on transition (-1/2, 5/2→1/2, 5/2) of the site 4 (Taylor and Farnell, 1964).

### B. Bleaching of Crystal

The F-centres in quartz, produced by the irradiation with electrons, neutrons, and X-rays, etc., are permanent at room temperature. However, they can be removed completely by heating up to a certain temperature or by ultra-violet irradiation. The required temperature and wave length

depend on the agency by which the centres were produced.

The bleaching agent employed in this research was heat. The sample was placed in a Central Scientific oven, which gives uniform temperature in the range from room temperature to 285°C, and which can also automatically adjust the temperature to a specified value. As the number of centres decreases, the temperatures required for bleaching increase. The bleaching was started at 150°C. Since the darkening depth depends on the energy and length of time of irradiation, it seems likely that the bleaching starts on the outside and moves inward. In this work, the temperature rose only to 224°C, due to the fact that gradual decrease of centres above this temperature is so small that the EPR signal could not be detected. The writer attempted to maintain a constant temperature, varying the time for bleaching. It was found that the EPR signal intensity versus time for bleaching, follows approximately the exponential function, as the alkali halide salt centre does.

Two methods were used to estimate the number of F-centres. First, the EPR line height and width were compared with those of a 0.5% $K_3Cr(CN)_6$ upper line, which was then compared with a weighed DPPH sample. Once the widths and heights of these lines are known, the number of F-centres can be calculated from the formula from Yaris et al (1961),

$$\frac{N^{(1)}}{N^{(2)}} = \frac{g_{\parallel}^{(1)} g_{\perp}^{(2)2} \Delta H^{(1)} \dfrac{2S^{(1)}+1}{(S^{(1)}+M^{(1)})(S^{(1)}-M^{(1)}+1)}}{g_{\parallel}^{(2)} g_{\perp}^{(1)2} \Delta H^{(2)} \dfrac{2S^{(2)}+1}{(S^{(2)}+M^{(2)})(S^{(2)}-M^{(2)}+1)}}$$

for the transitions from M $\longrightarrow$ M-1, where the (1) and (2) refer to the samples (1) and (2). Since the line width and height depend upon the

orientation of the crystals, errors may be introduced during different concentration-determination runs, due to the difficulty of placing the quartz and the potassium chromicyanode at the same angle for a specific axis in the D. C. field. The second method is to use a Perkin Elmer 350 photometer to measure the absorption coefficient of the colour centres. This method gives only relative concentrations. If the relation between number of colour centres and the absorption coefficient of light of a specific wave length is known, the actual number of colour centres can be estimated. However, due to the opacity of the smoky quartz during most of the concentration-determination runs, only a few measurements were carried out for this comparison. Since the EPR signal could not be detected after the smoky quartz became transparent, no relation between the reading obtained with the absorption coefficient and the actual colour centre concentration was found.

C. Measurement Method

There are two methods in general use for spin-lattice relaxation time measurement, namely, the CW saturation method and the pulse method. The CW saturation method, which is the method employed in this thesis and which is based on assumptions valid only in ideal cases, is not very reliable. The pulse method is limited to a relaxation time longer than of the order of one micro-second, and much greater power is usually required to saturate the sample.

If the attenuators before and after the cavity are adjusted so that the power going to the rf pre-amplifier is not great enough to

saturate the rf amplifier, and if the modulation is sufficiently reduced, the output signal is proportional to the power input to the cavity. That is, the deflection of the recorder needle is nearly proportional to $\frac{d\chi''}{dH}$ or $\frac{d\chi''}{d\omega}$

$$S \quad \frac{d\chi''}{d\omega} = \frac{\pi}{2}\chi_0 \nu \frac{d}{d\omega}\left[Z g(\omega)\right] = D \frac{d}{d\omega}\left[Z g(\omega)\right] \qquad \text{(V-1)}$$

where $Z = \dfrac{1}{1 + \frac{1}{2}\gamma^2 H_1^2 T_1 T_2}$ is the so-called saturation factor dependent upon the power, and g(w) is the line shape function; $\frac{w}{2\pi}$, the modulation frequency is here in the audio-frequency range, $H_1$ the magnitude of A. C. magnetic field; $\gamma$, the electron gyro-magnetic factor defined by $\gamma = \frac{ge}{2mc}$ and $T_2$ the spin-spin relaxation time defined by $T_2 = \frac{1}{2}\, g(w)_{max}$.

In all the measurements, $\omega_m T_1 \geq 6$ holds if the modulation frequency is 200 cycles/sec, then $W_m T_1 = 2\pi$. Enough accuracy is obtained by applying the condition $\omega_m T_1 >> 1$. Weissfloch (1963) has given the theoretical plotting of 20 log S against 10 log$\sigma$, and has shown that there is only a small divergence from that assumed $T_1 \omega_m >> 1$. From Andrew (1955), the output for a Lorentzian line is

$$S \propto \frac{(16+16\sigma+\sigma^2)^{\frac{1}{2}} - 2 - \sigma}{8+8\sigma-\sigma^2+(\sigma+2)(16+16\sigma+\sigma^2)^{\frac{1}{2}}} \qquad \text{(V-2)}$$

where $\sigma = \gamma^2 H_1^2 T_1 T_2$, parameter depends on power input.

Relative values of 20 log S and S are plotted against 10 log$\sigma$ respectively in figures 3 and 4. For the case $\sigma >> 1$, equation (V-2) can be expanded in terms of $1/\sigma$, neglecting terms of order higher than two, one gets the asymptotic line corresponding to figure 3, 20 x log S = const. + 2 x 10 log$\sigma$. Thus the asymptotic tangent is 2 and intersects

the abscissa, i. e. 10 log$\sigma$, at 1.6 db which can be easily verified. In the other graphs, (figure 4) the increase in power above a certain limiting level has very little effect.

For Gaussian line shape

$$g(\omega) = T_2 \, e^{-\frac{T_2^2}{\pi}(\omega_o - \omega)^2} \tag{V-3}$$

Since $T_1\omega_m >> 1$, Z cannot change during a modulation cycle, and the values of Z can be taken out of the bracket in equation (V-1). After straightforward calculation, we have

$$S \propto \frac{e^{-2a}}{2a} \qquad T_1\omega_m >> 1 \tag{V-4}$$

where a is a parameter defined as $\frac{T_2^2}{\pi}(\omega_o - \omega)^2 = a$ and which depends on $\sigma$ through the relation $1 + \sigma e^{-a} = 2a$. The same kind of plot is also given in figures 3 and 4. The general forms of these plots for the two kinds of line shapes appear to be very similar, with the exception of the first type of plot in which the asymptotic tangent is 1.9 and intersecting the abscissa at 2.5 db (Smith 1961).

Smith (1961) has given the formula for both line shapes as

$$T_1 = \frac{\text{Antilog}(-\frac{N}{10})}{0.65\,\gamma^2 K\, T_2} \tag{V-5}$$

for Lorentzian line shape

where $K = \frac{H_1^2}{P_i} = \frac{8\pi Q_u(1-\Gamma)^2 m^2 a^2}{\omega V(c^2+n^2a^2)}$, $Q_u$ is the unloaded Q of the cavity, $\Gamma$ is the reflection coefficient, $\frac{\omega}{2\pi}$ the frequency of the micro-wave power, V the volume of the cavity at resonance, a, b, and c the dimensions of the cavity, and $T_2 = \frac{1}{\sqrt{3\pi}\,\Delta\nu}$ ; and

$$T_1 = \frac{\text{Antilog}(-\frac{N}{10})}{0.56\,\gamma^2 K T_2} \quad \text{for Gaussian line shape} \tag{V-6}$$

where $T_2 = \frac{1}{\sqrt{2\pi}\,\Delta\nu}$, the line width defined here is between the points of inflection.

The signal strength to be taken during the experiments was the maximum deflection of the recorder needle, and the corresponding S is defined

$$S = \frac{\text{Maximum magnitude of unsaturated smoky quartz signal}}{\text{Maximum magnitude of saturated smoky quartz signal}} \qquad (V\text{-}7)$$

Usually, the saturated signals are compared with that of barely saturated crystals, such as DPPH. The DPPH line, unfortunately, is in the midst of the smoky quartz spectrum, and the measurements made for saturation effects on the specified line were influenced by the smoky quartz lines. The writer has tried without success to find other samples to substitute for DPPH. The same EPR line was used both for relaxation time measurement, and as the standard line to replace hard saturated sample. Great care had to be taken in order to maintain the cavity input power at a level low enough to eliminate a saturation effect. The attenuators immediately before and after the magic T were then set to the readings for unsaturation and saturation in alternation, and the magnitude of the same line noted.

Two methods were used to analyse the experimental data, both of which should give equivalent results, although not with the same degree of accuracy.

In the first method, S defined in equation (V-7) shows that a small fluctuation during the saturation of the crystal causes a serious error. Since, in the first kind of plot,

$$D = 20 \log S = 20 \log s_1 / s_2 \qquad (V\text{-}8)$$

The fluctuation introduced due to $\Delta s$ is

$$|\Delta D| \leq 20 \left\{ \left| \frac{\Delta s}{s_1} \right| + \left| \frac{\Delta s}{s_2} \right| \right\} \qquad (V\text{-}9)$$

In most cases, $\Delta s$ was comparable with $s_1$, and $|\Delta D|$ would be fairly large. This fluctuation would make it impossible to give an accurate asymptotic tangent, and besides, the time required for a complete saturation run is rather long. It is difficult to keep the temperature constant for such an extended period so that this method of analysis is not suitable for temperature dependence runs.

Another method corresponding to the theoretical plot of figure 4 was first developed by Bloembergen (1948). The corresponding signal S is defined as the reciprocal of equation (V-7), the error introduced due to the fluctuation of the signals being relatively small, as can be seen through following equations.

$$D = \frac{s_2}{s_1} \tag{V-10}$$

$$|\Delta D| \leq \left|\frac{\Delta s}{s_2}\right| + \left|\frac{s_2 \Delta s}{s_1^2}\right| \tag{V-11}$$

where $s_1 \neq s_2$ and $\Delta s < s_2$. Thus the fluctuation of $\Delta D$ is fairly small.

A horizontal line XY is drawn on figure 5, the intersections of which with different saturated S versus 10 log$\sigma$ plots will give the same values of $S$, that is,

$$S_A = S_B = S_C = \cdots \tag{V-12}$$

where $S_A$, $S_B$, $S_C$ etc. are functions of the corresponding $\sigma_A$, $\sigma_B$, $\sigma_C$, etc., respectively. One possible solution of equation (V-12) is,

$$\sigma_A = \sigma_B = \sigma_C = \cdots \tag{V-13a}$$

$$(\gamma^2 H_1^2 T_1 T_2)_A = (\gamma^2 H_1^2 T_1 T_2)_B = (\gamma^2 H_1^2 T_1 T_2)_C = \cdots \tag{V-13b}$$

and we find the ratio of spin-lattice relaxation time to be

$$\frac{T_{1A}}{T_{1B}} = \left(\frac{H_{1B}}{H_{1A}}\right)^2 \frac{T_{2B}}{T_{2A}} \qquad \text{(V-14)}$$

To express the ratio of power as a difference in db below one watt and the spin-spin relaxation time, $T_2$, in terms of line-width, equation (V-14) becomes, if lines A and B etc. are of the same shapes,

$$\frac{T_{1A}}{T_{1B}} = \frac{\Delta H_A}{\Delta H_B} \text{ Anti log } \frac{\Delta Db}{10}$$

where $\Delta$Db = db of A - db of B. This method requires the temperature to maintain constant for a shorter time, since only a few points around the specified line at half saturation are enough to determine the curve shapes.

In the second method, a sample of known spin-lattice relaxation time was placed in the cavity simultaneously. During each run, measurements were made on both samples. In this research, a crystal of $K_3Cr(CN)_6$, which was used as a standard for concentration comparison, was placed in the cavity with the smoky quartz. The spin-lattice relaxation time of the former crystal with a concentration $4 \times 10^{19}$ spins/c.c. served as a standard; it had been obtained by the first analytical method, where N was found by fitting the experimental data to the theoretical plot, being then calculated by equation (V-5).

Except for the highest concentration sample, all the spin-lattice relaxation times were analysed by the second method.

## VI. Experimental Results

A. Spin-spin relaxation time measurements were made at extremely high and low concentrations during this research. Since the spin-spin relaxation time $T_2$ relates to both the line shape and width, an accurate measurement on line width was carried out by counting the number of clicks of the D. C. magnetic field sweeping rate marker, this was calibrated to an accuracy of three significant figures with a Harvey Wells precision NMR gaussmeter. In order to determine the line shape, theoretical plots of both normalized Gaussian line and normalized Lorentzian line were fitted to the experimental curve. They were neither ideal Lorentzian nor Gaussian lines but were close to Lorentzian lines (see figures 6 and 7). This result contradicts that of Taylor who found that the line shape is closer to Gaussian line shape, the F-centre concentration of the crystals used by Taylor and this writer were of the same order. In general, we can say that as the concentration decreases, the line shape has a tendency to become closer to the Lorentzian line.

The line width of the sample at a high concentration i.e. $4 \times 10^{19}$ spins/c.c. is 0.65 gauss. Hence we have

$$T_2 = \frac{2}{\sqrt{3}\gamma\Delta H} = 5.5 \times 10^{-8} \text{ sec} \qquad \text{for Lorentzian line}$$

$$T_2 = \frac{\sqrt{2\pi}}{\gamma\Delta H} = 1.4 \times 10^{-7} \text{ sec} \qquad \text{for Gaussian line}$$

where $$\gamma = \frac{ge}{mc} = 1.75 \times 10^{7} \text{ gauss-sec.}$$

The line width of the extremely dilute sample, i.e. $2.8 \times 10^{18}$ spins/c.c. is 0.52 gauss, the corresponding spin-spin relaxation time being

$$T_2 = 6.6 \times 10^{-8} \text{ sec} \qquad \text{for Lorentzian line}$$

$$\text{and} \quad T_2 = 1.7 \times 10^{-7} \text{ sec} \qquad \text{for Gaussian line}$$

Additional measurements are necessary to find the corresponding spin-lattice relaxation time. From equations (V-5) and (V-6), there are four unknown quantities to be determined. The unloaded Qu was measured by the using of a ratio meter. Simultaneously, the coupling coefficient $\beta$, which is related to the reflection coefficient $\Gamma$, was also measured in under-coupled conditions. $\omega$ is the frequency of microwave power source and V the volume of the cavity at resonance. The numerical values of those quantities are given below

$$\beta = 0.63 \qquad \text{at } 4.2^\circ\text{K}$$

$$Qu = (1 + \beta)\, Q_L = 1.63 \times 3100 = 5100 \qquad \text{at } 4.2^\circ\text{K}$$

$$\omega = 2\pi \times 9.400 \times 10^9 \text{ sec}^{-1}$$

$$V = abc = 2.2 \times 1.0 \times 4.6 = 10 \text{ cm}^3$$

where $Q_L$ is the measured loaded Q of the cavity. The reflection coefficient $\Gamma = \frac{1 - \beta}{1 + \beta} = 0.23$. Then we have

$$K = \frac{H^2}{P_i} = 0.98$$

The experimental data for S were fitted to the theoretical plot of figure 4, from which one finds the intersection of the asymptotic line with the abscissa at 50.4 db (=N) as shown in the typical plot of this kind in figure 8.

At 4.2°K, by equations (V-5) and (V-7), for the $4 \times 10^{19}$ spins/c.c. case, N = 50.4 db, we have

$$T_1 = 10 \times 10^{-3} \text{ sec} = 10 \text{ ms} \qquad \text{for Lorentzian line}$$

and

$$T_1 = 4.8 \text{ ms} \qquad \text{for Gaussian line}$$

B. Temperature Dependence

In this and next sections, experimental data were analysed by the second method described in section (V-C). A typical plot of this kind was shown in figure 9 for the concentration of $4 \times 10^{19}$ spins/c.c. The reading for S = 0.5 on input power below one watt at 3.4°K subtracted from the reading for S = 0.5 on input power below one watt at 4.2°K, gives $\Delta$Db = 2.3 db. Since $T_1$ at 4.2°K is known, and the line-widths at 4.2°K and 3.4°K are almost the same, the spin-lattice relaxation time $T_1$ at 3.4°K can be calculated from equation (V-15).

Figures 10 and 11 show how the spin-lattice relaxation time depends on temperature. The temperatures in the range from 4.2°K to 1.6°K were achieved by pumping liquid helium in the inner dewar. By means of a temperature and vapour pressure correspondence chart, which is calibrated by a thermocouple, the temperature can be read directly from the readings on the manometer. However, since hydraulic pressures were not indicated during the calibration, it is difficult to know the true temperature of the sample merely from the pressure readings, when the temperature is between 4.2°K and 2.2°K, the $\lambda$ point of liquid helium. Because the walls of the dewar are at a different temperature from the surface of the liquid helium, a temperature gradient exists and, obviously, the temperature difference between the sample and the liquid helium surface depends on the height of the latter. In most cases, the

amount of liquid helium poured into the dewar cannot be controlled accurately. Below the $\lambda$ point, liquid helium becomes a superfluid, therefore the temperature gradient no longer exists. Hence the accuracy of readings at temperatures above 2.2°K would not be as great as those made below the $\lambda$ point.

Figures 10 and 11 confirm the existence of two processes, supposedly dominating in two regions separated by a certain temperature, the "critical temperature", which depends on the concentration of F-centres. As the concentration decreases, the "critical temperature" increases. One process, dominating below the "critical temperature" results in the spin-lattice relaxation time to be proportional to $T^{-0.7}$; while the other process, taking place when the temperature is above the "critical temperature", gives $T_1 \propto T^{-2.6}$.

Results of the spin-lattice relaxation time at two extremes of concentration, and at 4.2°K and 1.7°K, are presented both for Lorentzian and Gaussian line shapes as below:

| Concentration | Temperature | $\Delta$Db | $T_1$(ms) Lorentzian | $T_1$(ms) Gaussian |
|---|---|---|---|---|
| $4 \times 10^{19}$ spins/c.c. | 4.2° K | 0 | 10 | 4.8 |
| | 1.75° K | 6.0 | 42 | 18 |
| $2.8 \times 10^{18}$ spins/c.c. | 4.2° K | 14.5 | 296 | 127 |
| | 1.65° K | 20.3 | 1100 | 472 |

It has to be pointed out here that at $4 \times 10^{19}$ spins/c.c., both analytical methods were used at each temperature, showing that the results are consistent within experimental errors. For the lower concentrations, the second method only was employed.

C. Concentration Dependence

The relation of spin-lattice relaxation time to concentration is presented in figure 12. The useable concentration is no less than $2.8 \times 10^{18}$ spins/c.c., below which the EPR signal to noise ratio is so small that measurement of the EPR saturation effect becomes impossible.

By means of the least square method, an empirical expression was fitted to this data. Using McGill's IBM 7040 computer, one can get,

$$T_1 = 0.192 + 0.164 \times 10^1 c_s - 0.119 \times 10^2 c_s^2 + 0.262 \times 10^2 c_s^3 - 0.246 \times 10^2 c_s^4 + 0.848 \times 10^1 c_s^5$$

where $c_s$ is the number of F-centres in a unit of $4.0 \times 10^{19}$ spins/c.c. and $T_1$ the spin-lattice relaxation time in second.

As the concentration decreases, the spin-lattice relaxation time $T_1$ increases until $8 \times 10^{18}$ spins/c.c. is reached. Henceforward, $T_1$ proceeds to a certain limit, beyond which there is no corresponding increase with decrease in concentration.

Most of the measurements were made on the fifth line, i.e. $(-1/2, 3/2 \rightarrow 1/2, 3/2)$ of site 4. In several cases, measurements were also made on the sixth line, i.e. $(-1/2, 5/2 \rightarrow 1/2, 5/2)$ of the same site. The relaxation times for both lines at extremely high concentration are approximately equal. However, for very low concentration, they differ widely. It has been found that the spin-lattice relaxation time ratio for transition $(-1/2, 3/2 \rightarrow 1/2, 3/2)$ at the two extremes is 25, while that for the transition $(-1/2, 5/2 \rightarrow 1/2, 5/2)$ is 91, almost four times larger. The spin-lattice relaxation times for transition $(-1/2, 5/2 \rightarrow 1/2, 5/2)$

were obtained by both kind of analyses, the results being fairly consistent. Thus the inconsistency in ratio must be due to causes other than experimental error.

D. Line-width Variations with Concentration

At most concentrations, line-widths were measured at 4.2°K on transition (-1/2, 3/2 $\rightarrow$ 1/2, 3/2) of the site 4 using modulation of less than 0.1 gauss. However, due to the D. C. magnetic field sweeping rate being relatively too fast, no precise results can be presented. All that can be said is that the line-width decreases with decreasing concentration, and the ratio of the line-width of the fifth line at the greatest and least concentration is 0.65/0.52.

# VII. Discussion of Results

## A. Spin-lattice Relaxation Time

Measurements on spin-lattice relaxation time have been reported previously by several authors and each has shown some kind of inconsistency.

Carr and Strandberg (1962), using the CW saturation method, found that $T_1$ at 4.2°K was 300 ms and greater than 3 seconds at 1.7°K. They mentioned neither the concentration of crystals at which their measurements were carried out, nor the shape of the line obtained. From acoustic saturation data Taylor estimated that the concentration of the sample they used was less than $3.4 \times 10^{19}$ spins/c.c.

Using both the CW saturation technique and the pulse technique, Taylor (1963) carried out measurements on $T_1$ for X-cut smoky quartz of a concentration of $3.4 \times 10^{19}$ spins/c.c., in the temperature range 4.2°K to 1.6°K. His results are shown below:

| | $T_1$(ms) by CW saturation technique | | $T_1$(ms) by |
|---|---|---|---|
| Temperature | Lorentzian | Gaussian | pulse technique |
| 4.2°K | $3.9 \pm 1.5$ | $1.8 \pm 0.8$ | $34 \pm 5$ |
| 1.6°K | $15.4 \pm 6$ | $7.3 \pm 3$ | $125 \pm 15$ |

The difference in spin-lattice relaxation time as measured by the pulse and the CW saturation technique, he concluded, was due to both site-to-site and dipolar cross-relaxation.

Comparing Taylor's results with those obtained in this thesis, the former is smaller by half at 4.2°K. The concentrations are believed to be approximately of the same order.

B. Temperature Dependence

In both papers mentioned in the previous section, spin-lattice relaxation times have been measured at four different temperatures at least. In Carr and Strandberg's paper, measurements were made at 1.7°K, 4.2°K, 35°K and 77°K. Due to the temperature invervals being too large, no indication of process changes appeared. Even in Taylor's attempt to prove that neither a direct nor an indirect process exists in smoky quartz spin-lattice relaxation, the results of his measurements show that the relationship between $T_1$ and temperature is far from following the single process which would be important at very low temperatures. It is believed that further studies of temperature dependence at temperatures beyond 4.2°K will show more clearly which processes are actually in existence. Shamfarov and Smirnova (1963), using neutron-irradiated quartz at two different concentrations, found, by using the pulse inversion method, in the temperature range from 1.6°K to 4.2°K, that, both for the $10^{18}$ spins/c.c. sample in the temperature range from 1.6°K to 3°K, and for the $10^{19}$ spins/c.c. sample in the temperature range from 1.6°K to 2°K, the spin-lattice relaxation time follows $T_1 \propto T^{-1}$ law; while from the temperatures indicated above to 4.2°K, the spin-lattice relaxation time follows $T_1 \propto T^{-4}$ law. This change in "critical temperature" from 3°K to 2°K with change of concentration might indicate a different relaxation mechanism at the different concentrations.

As shown in chapter III, the spin system in an excited state, is related to thermal equilibrium by two kind of processes. The direct process, usually dominant at a very low temperature, leads to $T_1$ proportional to $T^{-1}$.

The Raman, or indirect process, leads to $T_1$ proportional to $T^{-7}$. In figures 7 and 8, the spin-lattice relaxation time $T_1$ is proportional to $T^{-0.6}$ and $T^{-2.7}$ respectively.

From our results and those of Shamfarov et al, we may conclude that at temperatures below 3°K in highly concentrated crystals, the direct process dominates. A reading for $T_1$ proportional to $T^{-0.6}$ instead of $T^{-1}$ could not be simply due to experimental error, since the temperature measurement made below the $\lambda$ point, and the spin-lattice relaxation are fairly precise. For $T_1$, in a temperature range higher than 3°K, we could not determine whether it follows the $T_1 \propto T^{-7}$ law. Measurements made above 4.2°K will clarify this point. The spin-lattice relaxation time $T_1 \propto T^{-2.7}$ for temperatures above 3°K, does not seem to be contributed from the local mode of lattice vibration at the defect as shown by Castle el al (1963). If the local frequency $\omega_i > \omega_D$, the Debye frequency, the spin-lattice relaxation time will have a term proportional to $T^{-3}$. The conditions for $\omega_i > \omega_D$ are that either the mass of the impurity is less than that of the donor, or that the local strain is enhanced. This seems impossible in the case of aluminum as the impurity in quartz.

Klemens (1962) showed that at temperature $T_c = \frac{1}{2}\left(\frac{A}{B}\right)^{\frac{1}{3}}\left(\frac{E}{K\Theta}\right)^{\frac{2}{3}}$, the direct and Raman processes are comparable. In this experiment, $E/K = 0.46°K$, and for quartz, the Debye temperature measured by Jones and Hallis Hallet (1960) is 469°K. In most cases, $\left(\frac{A}{B}\right)^{\frac{1}{3}} \simeq 1$ so that $T_c \simeq 25°K$, which is much higher than the temperatures measured. This may

be due to Klemens, in his calculation, neglecting the factor contributed from the integral $\int_0^{\infty} \frac{x^6 e^x}{(e^x-1)^2} dx$. The Debye temperature may also be lower after the quartz is irradiated.

C. Concentration Dependence

So far there is no other reported result about spin-lattice relaxation time depending on concentration of smoky quartz. Taylor noted only that his results were not of the same order of magnitude as those of Carr and Strandberg, and he attributed these differences to crystals of different concentrations being used. Shamfarov and Smirnova also pointed out that the spin-lattice relaxation time measured of different concentrations had huge difference.

Since the Zeeman splittings of the smoky quartz are much greater than those of the hyperfine splittings, it is difficult to convert the Zeeman energy to energy produced by dipolar interaction, quadrapolar interaction, etc.; consequently, it is impossible to consider it as a single spin system. The rate of establishment of thermal equilibrium between the system of individual spin levels of the paramagnetic centres and the system of dipoles etc., will be characterized by the term of cross-relaxation time. On the other hand, interactions, which are not strong enough to split the energy levels but strong enough to broaden the resonant absorption lines, also contribute greatly to cross-relaxation. In the case of smoky quartz, the separation of two neighbouring lines is so small compared to their line-widths that overlapping is impossible to avoid. Thus cross-relaxation plays an important role

in the relaxation mechanism.

From the observed electron-spin-resonance absorption spectra, we know that dipole-dipole interaction is quite strong in smoky quartz. For a given crystal, the distance between two nearest centres, i and j, is proportional to the inverse cube root of the number of centres contained i. e., $r_{ij} = N^{-1/3}$. Since the dipole-dipole interaction is proportional to $r_{ij}^{-3}$, it will be directly proportional to the number of centres in the specified crystal. The cross-relaxation time is defined as $T_{21} = \left[2\frac{2\pi}{k}\left|\langle 2|\mathcal{H}_{dipole}|1\rangle\right|^2 f\right]^{-1}$, thus the cross-relaxation time $T_{21}$ is inversely proportional to the square of concentration. To express the number of centres in units of $4 \times 10^{19}$ spins/c.c., which seems to be the highest concentration one can get with the sample used, thus one has $T_{21} = c_s^2$.

The empirical formula has terms of order up to the fifth power of concentration, and the coefficients of $c_s^2$, $c_s^3$, $c_s^4$, are of the same order of magnitude. This conflict between the experimental results and the simple estimation of the previous paragraph may be due to other interactions which the writer has ignored. Since the lattice is vibrating, the distance between the centres is not a constant. Thus the dipole-dipole interaction cannot be so represented as in the sixth term of equation (III-2); and usually, $B_k$ is also a function of spacial coordinates. Hence the result will be more complicated.

Lastly, it is worth noting that with decrease in concentration, the more rapid increase of $T_1$ on the $(-1/2, 5/2 \rightarrow 1/2, 5/2)$ line as compared with $T_1$ on the $(-1/2, 3/2 \rightarrow 1/2, 3/2)$ line is due to the energy of

the latter being more easily shared by its immediate energy level than that of the former, since the energy involved in the transition (- 1/2, 3/2 → 1/2, 3/2) is nearer to the average energy of the whole site. Consequently, we should expect a stronger dependence of concentration for the lines (- 1/2, 1/2 → 1/2, 1/2) and (- 1/2, - 1/2 → 1/2, - 1/2) than for any of the other lines in the same site.

## VIII. Conclusions

Measurements were made on the $(-1/2, 3/2 \rightarrow 1/2, 3/2)$ line of site 4 of the X-cut smoky quartz, especially of the spin-lattice relaxation time dependence on concentration and on temperature. The experimental results are summarized as follows:

(1) The spin-lattice relaxation time of a crystal with concentration $4 \times 10^{19}$ spins/c.c. at 4.2°K is 5 to 10 milli-seconds.

(2) Temperature dependence measurements of $T_1$ were carried out for four different concentrations in the temperature range from 4.2°K to 1.6°K. Two different processes are in dominance in the temperature regions separated by 3°K, for $1.6 \leq T \leq 3$°K, $T_1 \propto T^{-0.7}$ and $T \geq 3$°K, $T_1 \propto T^{-3}$.

(3) Spin-lattice relaxation time, $T_1$ was measured as a function of concentration from $4 \times 10^{19}$ spins/c.c. to $2.8 \times 10^{18}$ spins/c.c. An empirical formula was found by the method of least square.

$$T_1 = 0.192 + 0.164 \times 10^{1} c_s - 0.119 \times 10^{2} c_s^2 + 0.262 \times 10^{2} c_s^3 - 0.246 \times 10^{2} c_s^4 + 0.848\ 10^{1} c_s^5$$

where $c_s$ is the concentration in units of $4 \times 10^{19}$ spins/c.c. and $T_1$ in seconds.

## References


Abragam, A., (1961), The Principles of Nuclear Magnetism, (Oxford: Clarendon Press).

Andrew, E. R,, (1955), Nuclear Magnetic Resonance, (Cambridge University Press).

Bloembergen, N., (1948), Nuclear Magnetic Resonance, (Benjamin Inc.).

Carr, P. H. and Strandberg, M. W. P., (1962), J. Chem. Phys. Solids, 23, 923.

Castle Jr., J. G., Feldman, D. W. and Klemens, P. G., (1963), Phys. Rev., 130, 577.

Feldman, D. W., Warren, R. W. and Castle Jr., J. G., (1964) Phys. Rev., 135, A470.

Feher, G., (1957), Bell System Tech. J., 36, 449.

Heitler, W., (1944), Quantum Theory of Radiation, (Oxford University Press).

Heitler, W. and Teller, E., (1936), Proc. Roy. Soc., A155, 629.

Griffiths, J. H. E., Owen, J. and Ward, I. M., (1954), Nature, 173, 439.

Griffiths, J. H. E., Owen, J. and Ward, I. M., (1955), Defects in Crystalline Solids, (London, Physical Society).

Jones, G. H. S. and Hallis Hallett, A. E., (1960), Can. J. Phys., 38, 696.

Klemens, P. G., (1962), Phys. Rev., 125, 1795.

Kronig, R. de L., (1939), Physica, 6, 33.

Lortie, M. H., (1960), M. Sc. Thesis, McGill University, (Unpublished).

Mattuck, R. D. and Strandberg, M. W. P., (1960), Phys. Rev., 119, 1204.

O'Brien, Mary C. M., (1955), Proc. Roy. Soc., A231, 404.

Orbach, R., (1961), Proc. Roy. Soc., A264, 458.

Shamfarov, Ya. L. and Smirnova, T. A., (1963), Soviet Phys.-Solid State, 5, 761.

Smith, P., (1961), M.Sc. Thesis, McGill University, (Unpublished).

## References

Taylor, A. L., (1963), Ph. D. Thesis, McGill University, (Unpublished).

Taylor, A. L. and Farnell, G. W., (1964), Can. J. Phys., 42, 595.

Van Vleck, J. H., (1940), Phys. Rev., 57, 426.

Waller, I., (1932), Z. Physik, 79, 370.

Wei P'ei-Hsiu, (1935), Z. Krist., 92, 355.

Weissfloch, C., (1963), M. Sc. Thesis, McGill University, (Unpublished).

Yariv, A. and Gordon, J. P., (1961), Rev. Sci. Instr. 32, 462.

Ziman, J. M., (1960), Electrons and Phonons, (Oxford; Clarendon Press).

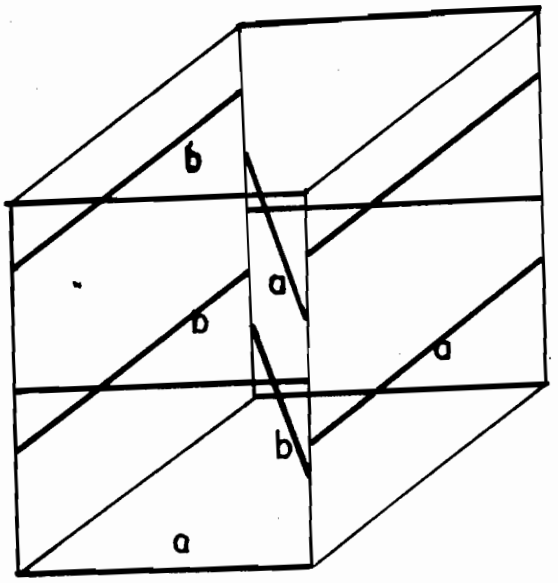


(a)

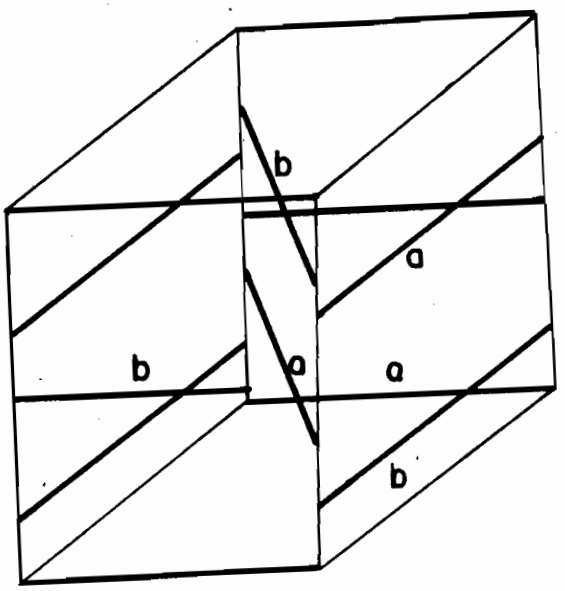


(b)

FIG. 1

Diagram 1a. shows space group $D_3^6$, 1b. shows space group $D_3^4$, heavy lines represented two-fold axes.

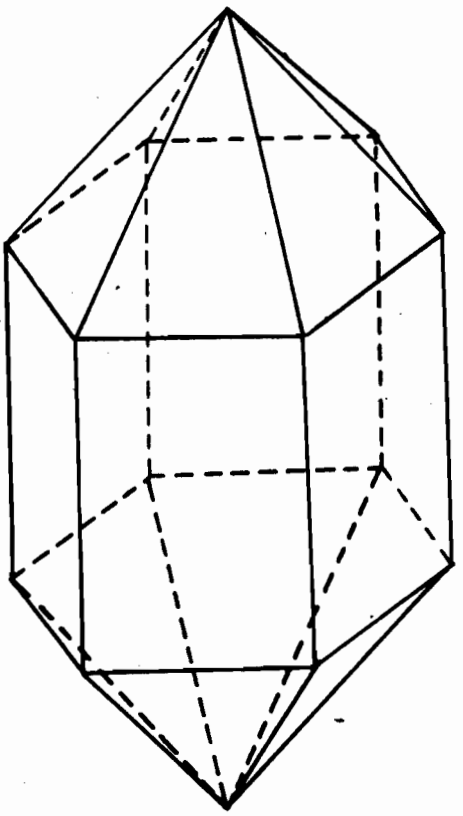

(a) α-quartz

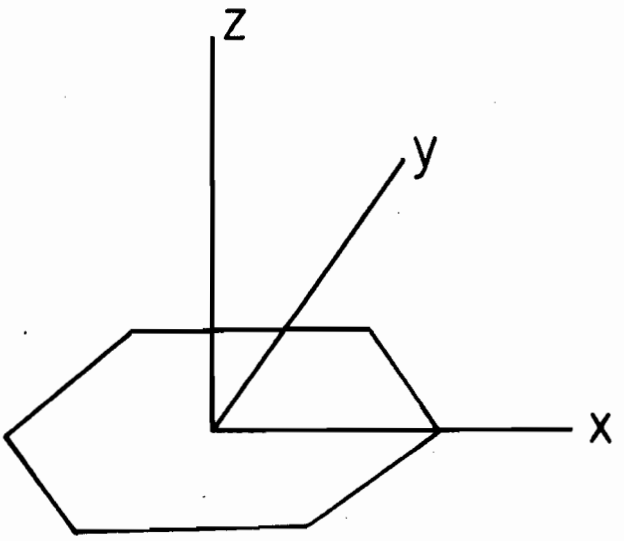


(b) Axes

FIG. 2

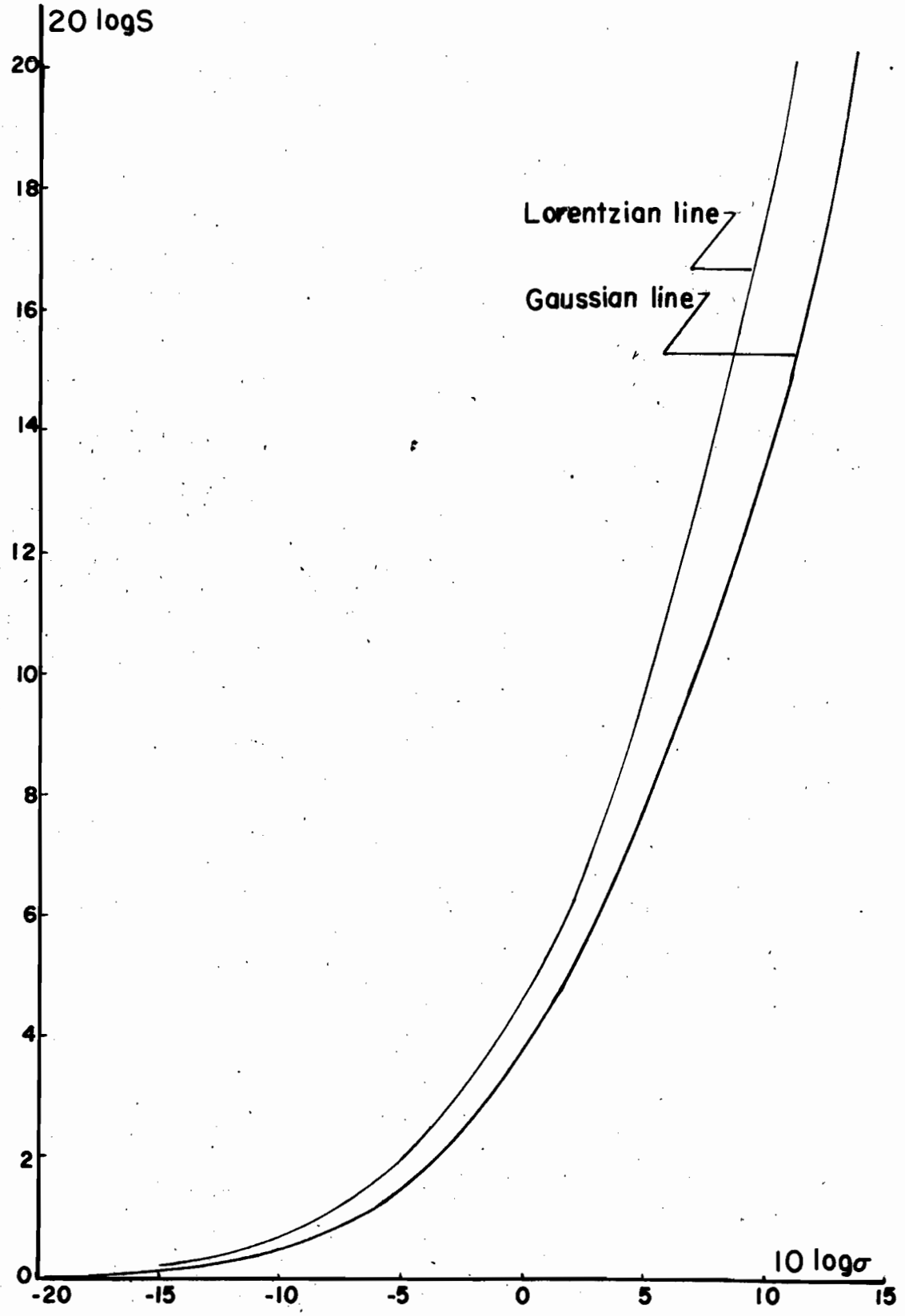


FIG. 3

Theoretical saturation curves for $T_1\omega_m \gg 1$

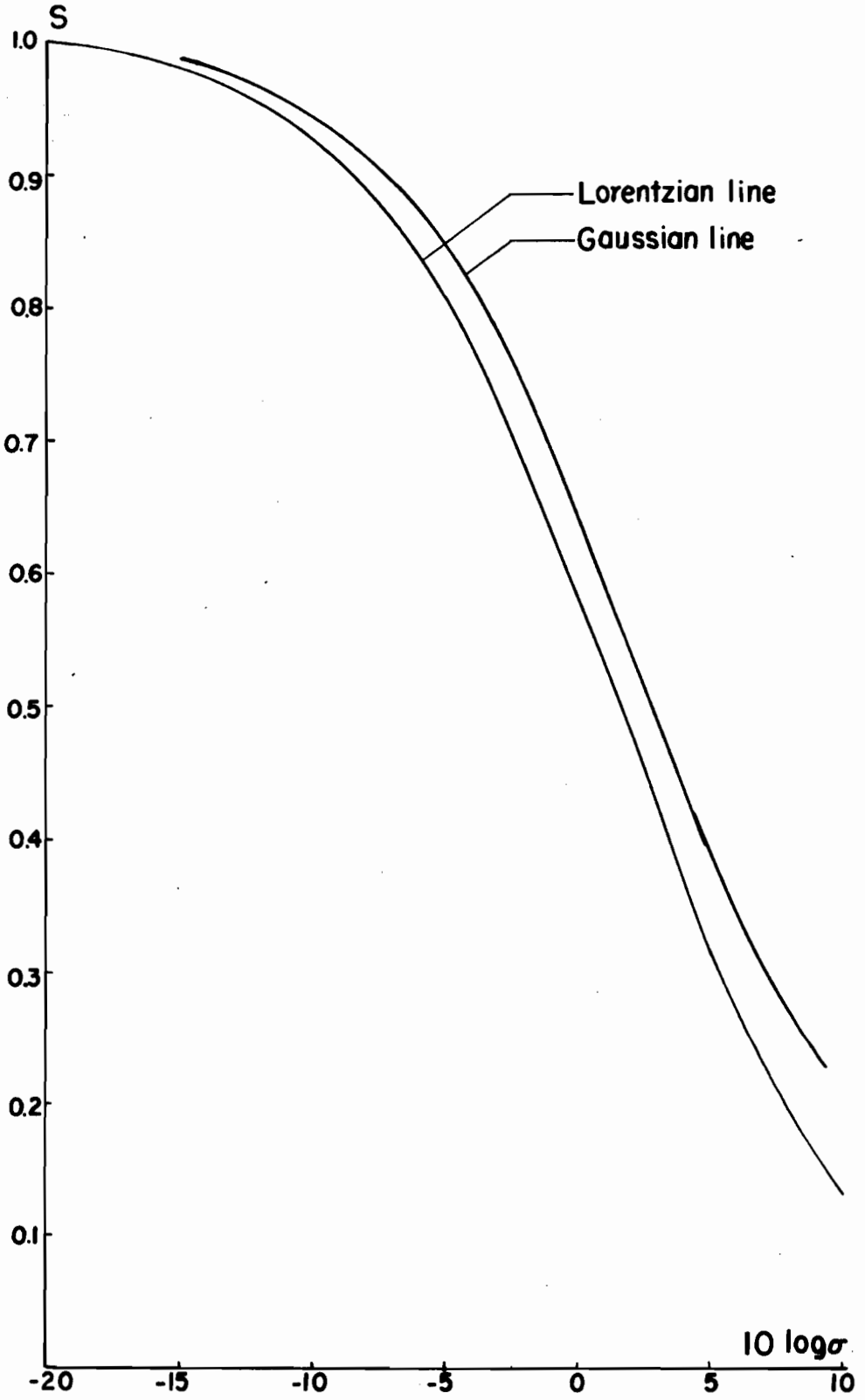


FIG. 4

Theoretical saturation curves for $T_1 \omega_m \gg 1$

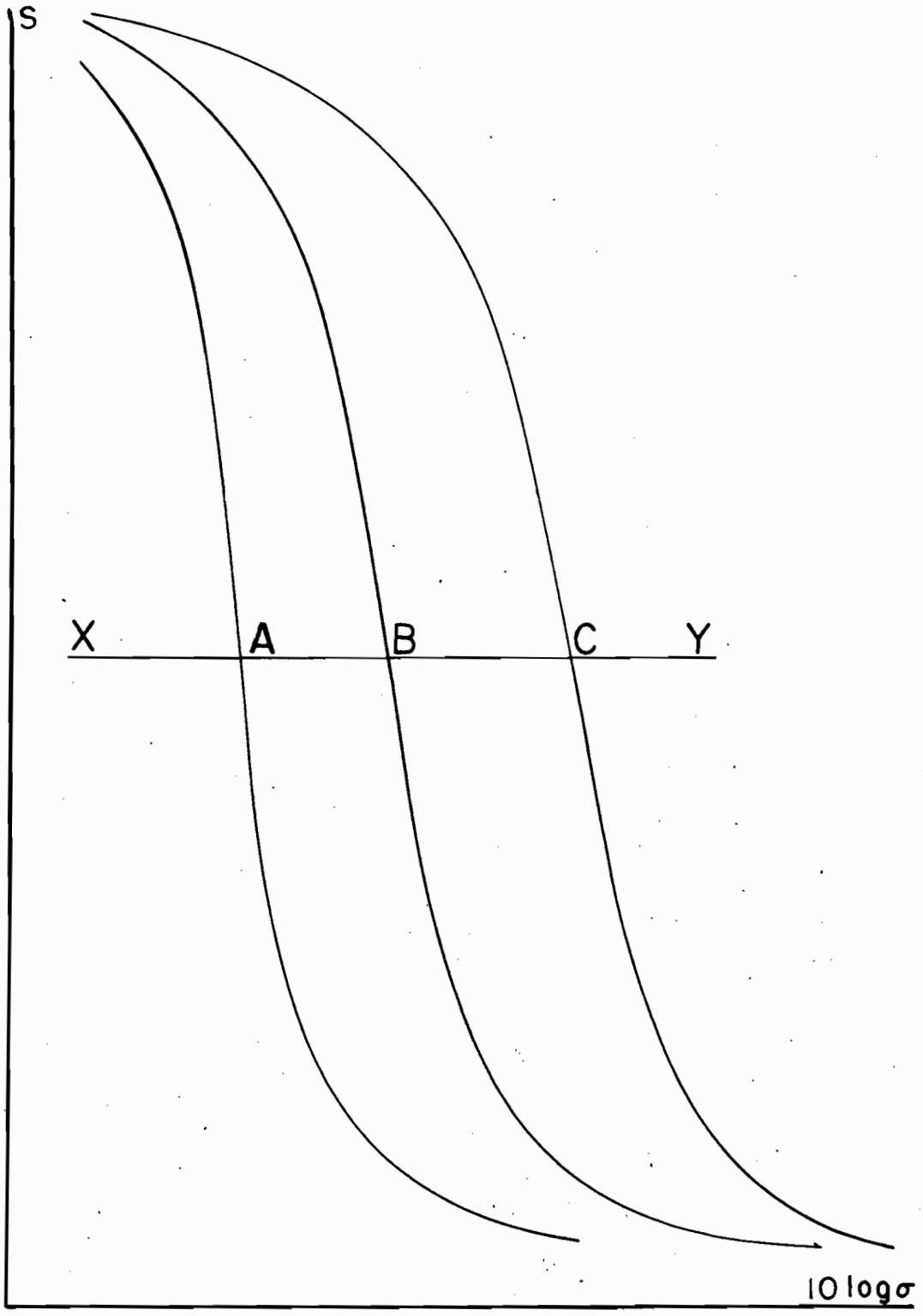


FIG. 5

Theoretical saturation curves correspond to different temperatures or samples

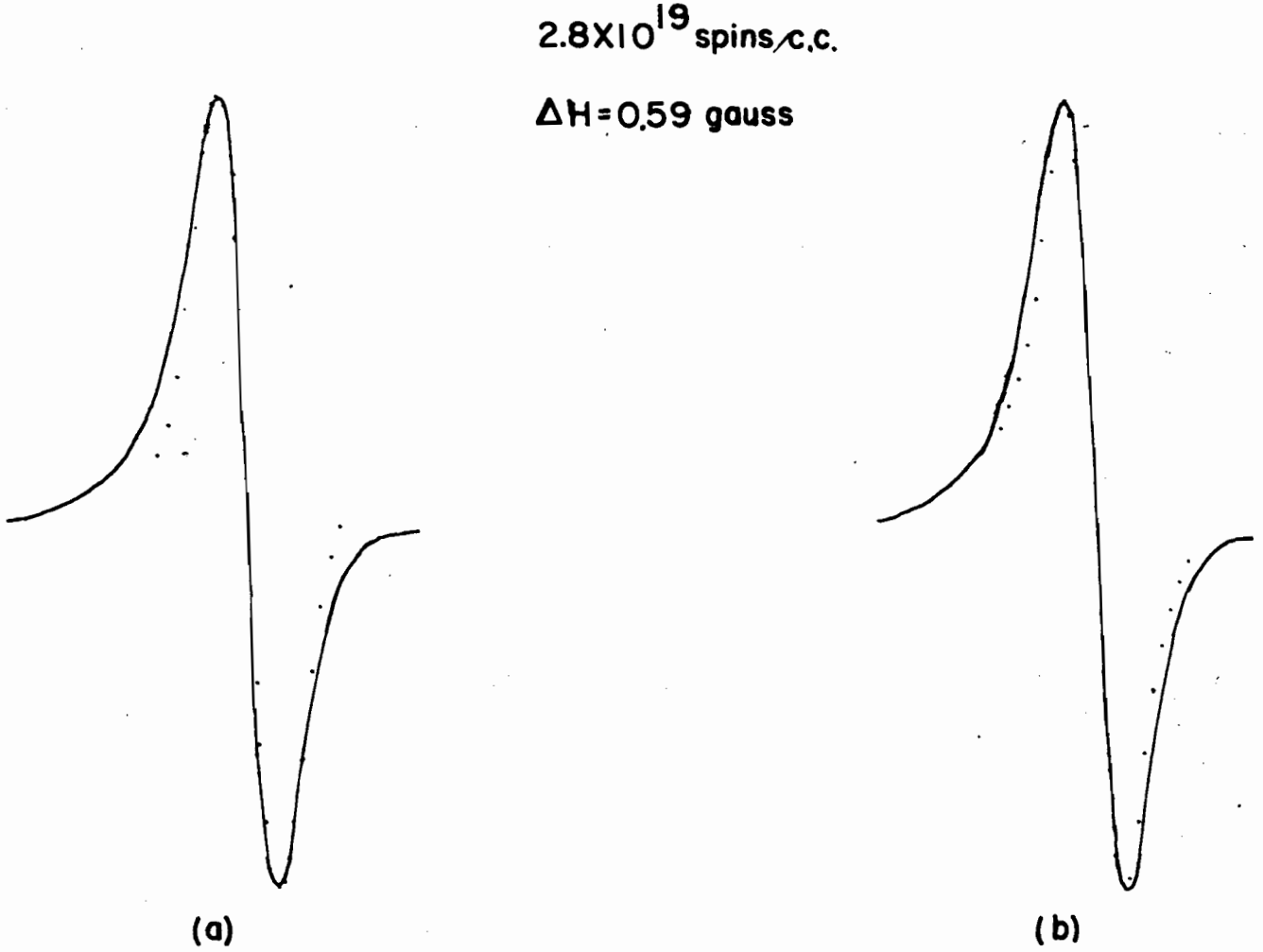


FIG. 6

Comparisons of experimental curve with (a) Gaussian line (b) Lorentzian line

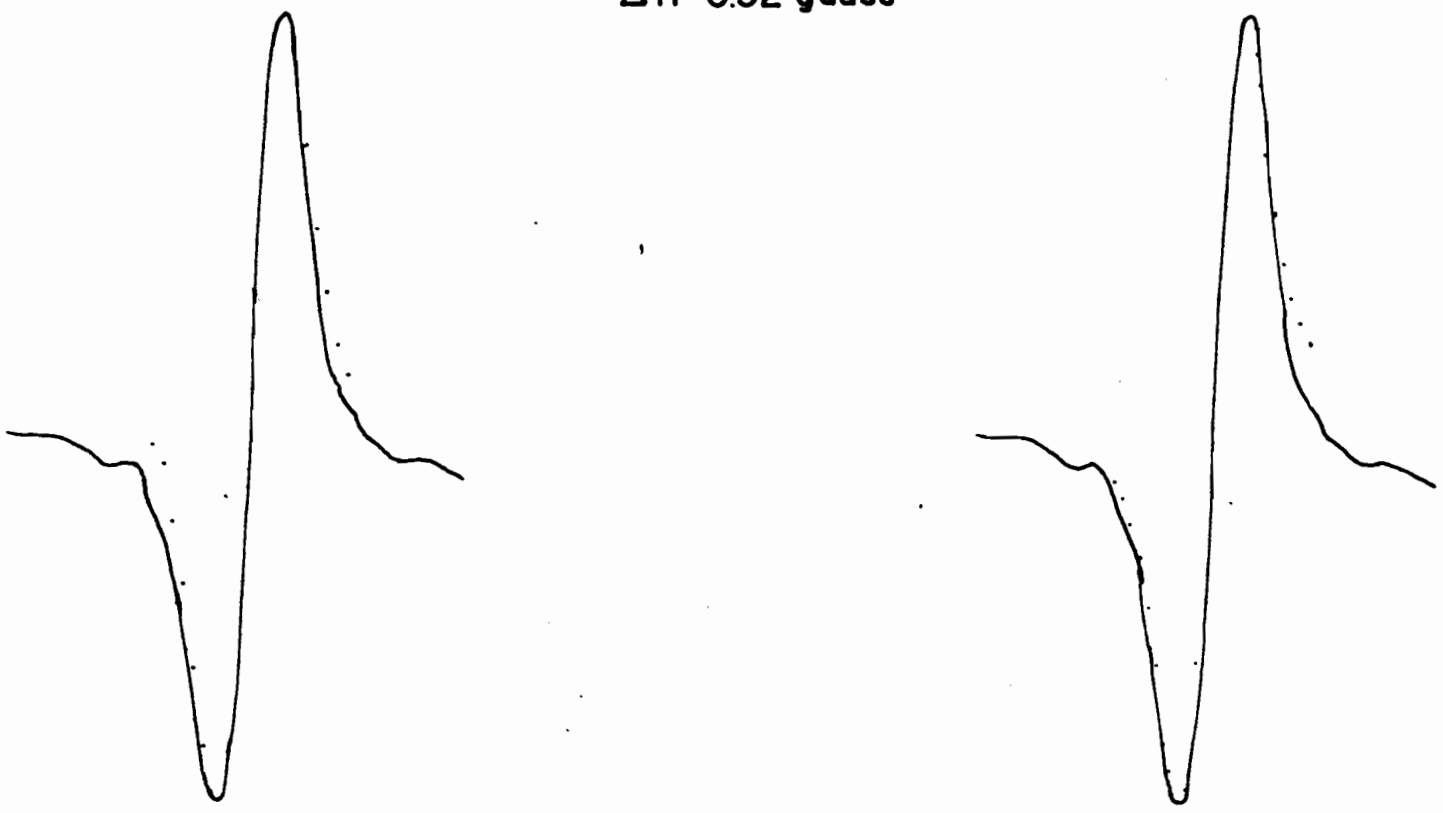


FIG. 7

Experimental curve compared with ideal (a) Gaussian line (b) Lorentzian line

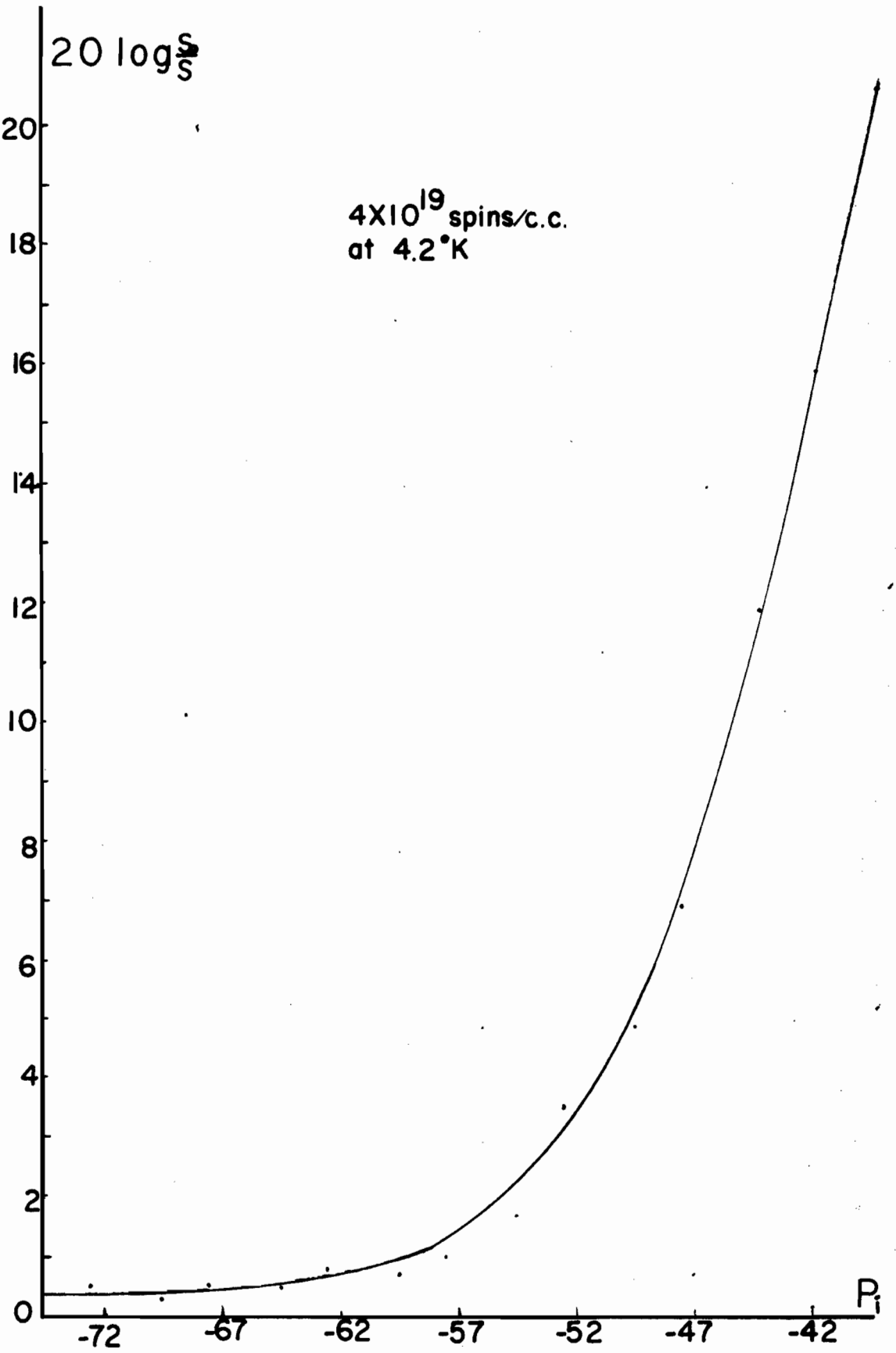


FIG. 8

Experimental saturation curve

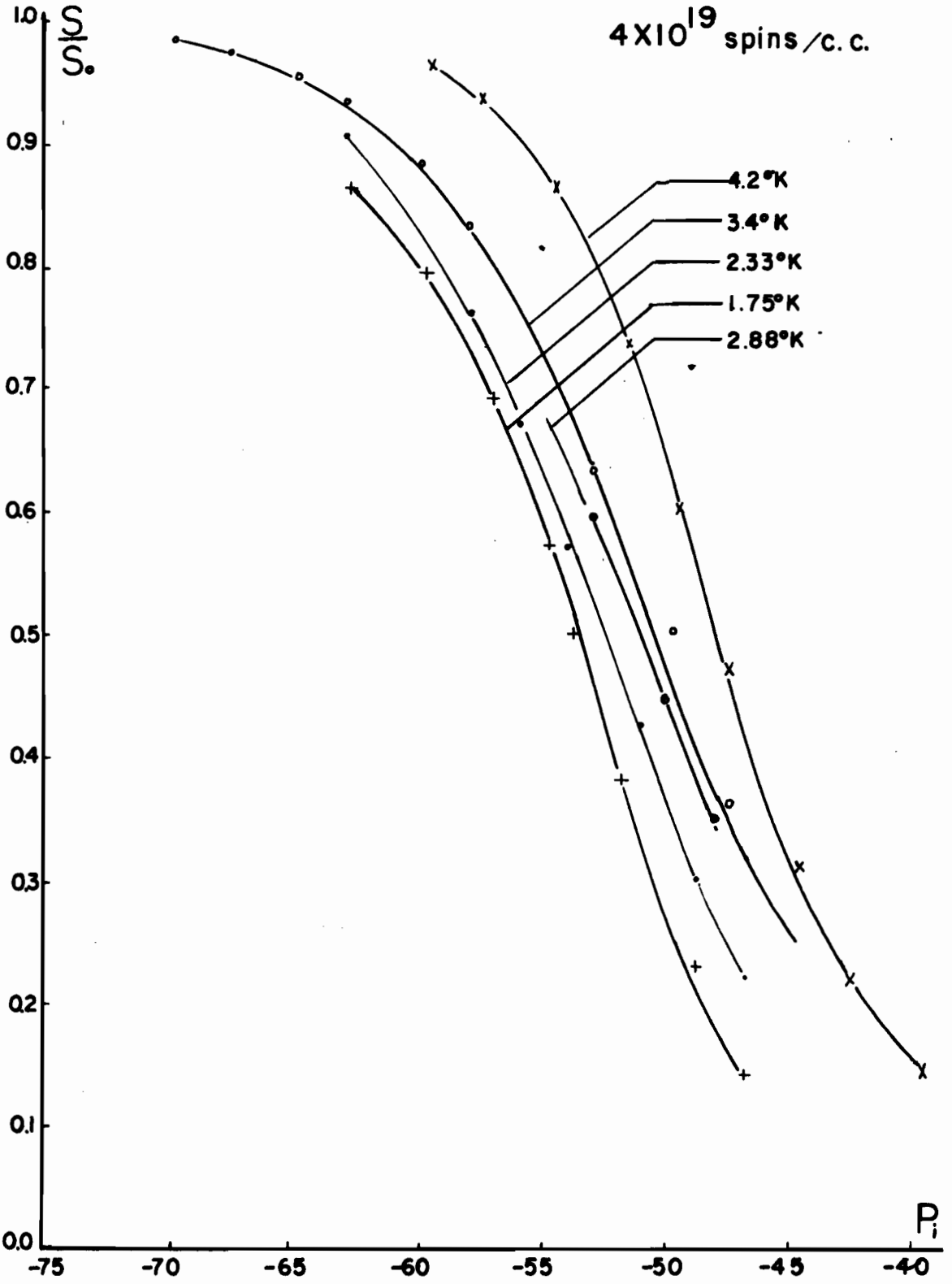


FIG. 9

Experimental saturation curves at different temperatures

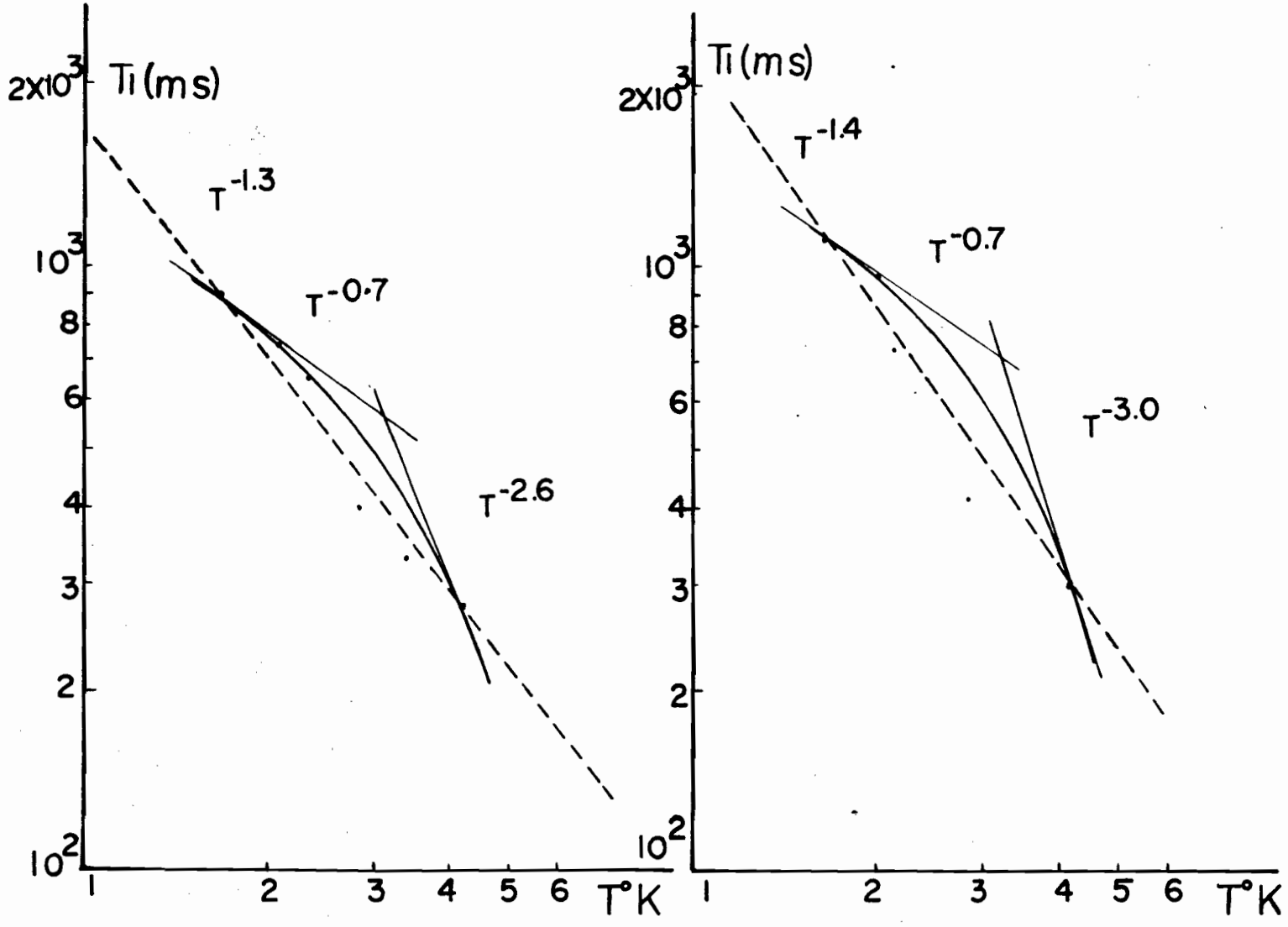


FIG 10 Temperature Dependence

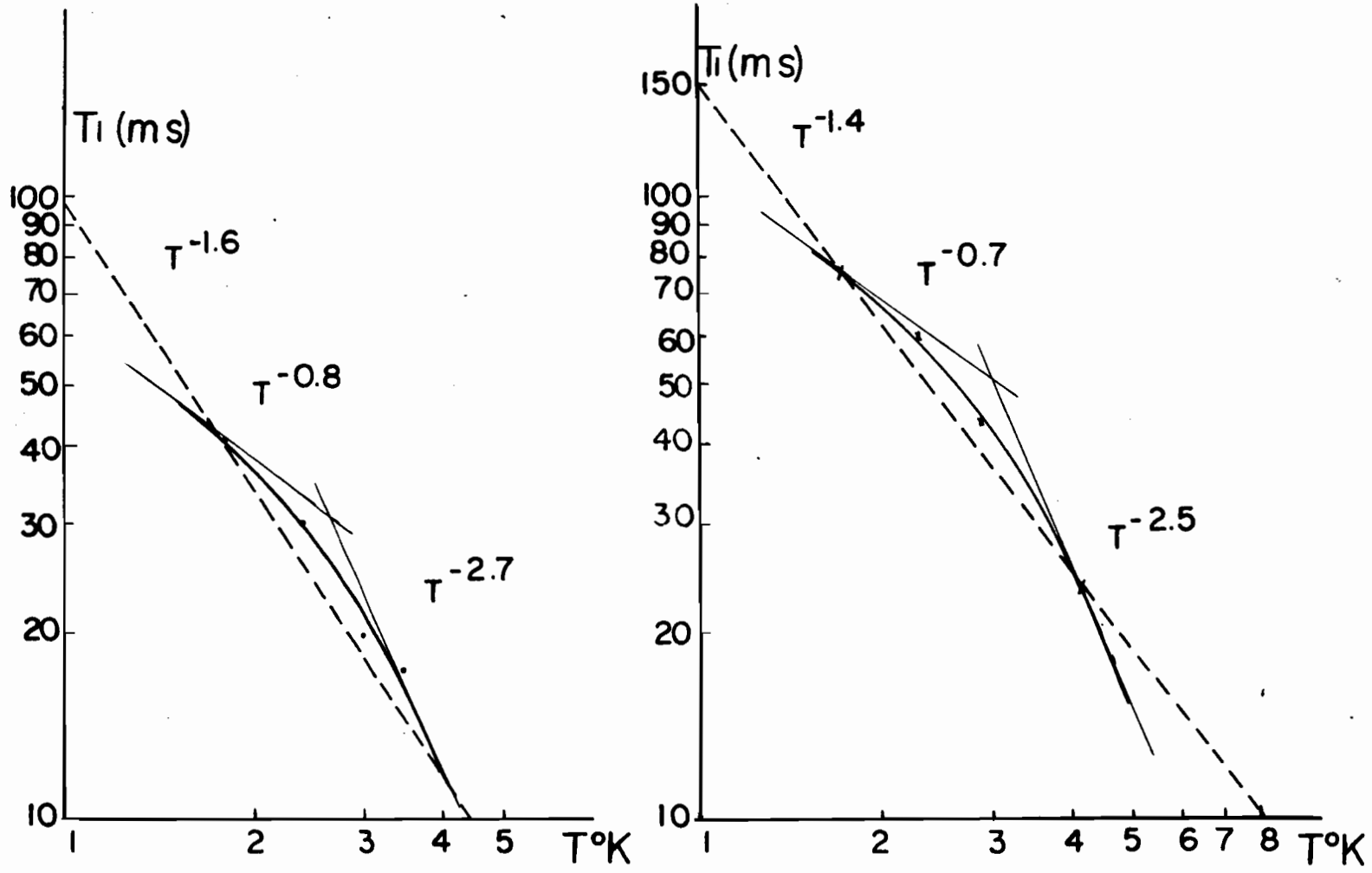


FIG. 11 Temperature Dependence

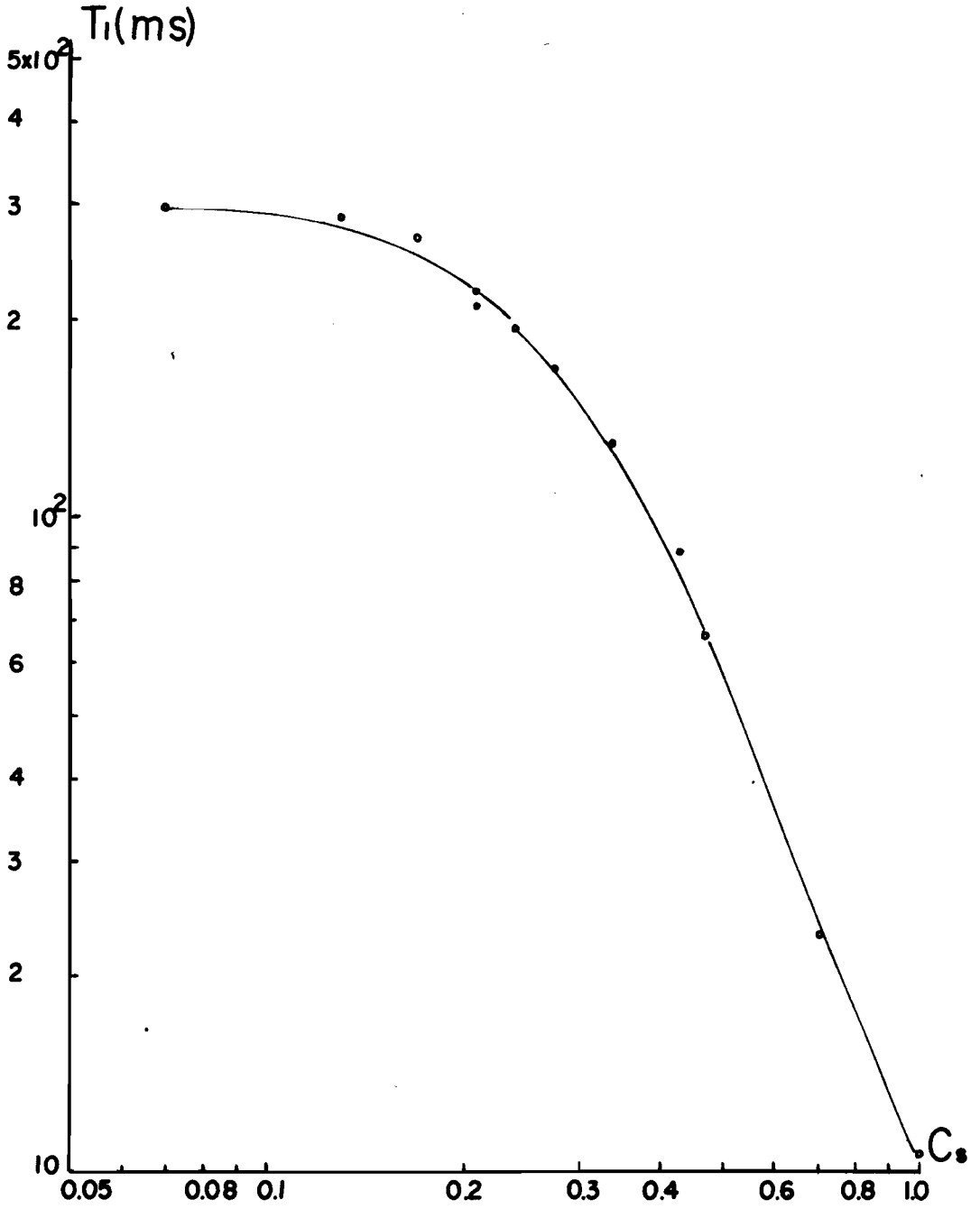


FIG. 12 Concentration Dependence